

AUTHOR QUERY FORM

 ELSEVIER	Journal: JNDT Article Number: 1176	Please e-mail or fax your responses and any corrections to: E-mail: corrections.esch@elsevier.macipd.com Fax: +44 1392 285878
--	---	--

Dear Author,

Any queries or remarks that have arisen during the processing of your manuscript are listed below and highlighted by flags in the proof. Please check your proof carefully and mark all corrections at the appropriate place in the proof (e.g., by using on-screen annotation in the PDF file) or compile them in a separate list.

For correction or revision of any artwork, please consult <http://www.elsevier.com/artworkinstructions>.

Articles in Special Issues: Please ensure that the words ‘this issue’ are added (in the list and text) to any references to other articles in this Special Issue

Uncited references: References that occur in the reference list but not in the text – please position each reference in the text or delete it from the list.	
Missing references: References listed below were noted in the text but are missing from the reference list – please make the list complete or remove the references from the text.	
Location in article	Query/remark Please insert your reply or correction at the corresponding line in the proof
	No queries

Electronic file usage

Sometimes we are unable to process the electronic file of your article and/or artwork. If this is the case, we have proceeded by:

Scanning (parts of) your article Rekeying (parts of) your article Scanning the artwork

Thank you for your assistance.



ELSEVIER

Contents lists available at ScienceDirect

NDT&E International

journal homepage: www.elsevier.com/locate/ndteint

Assessment of metal strand wire pre-stress in anchor head by ultrasonics

D. Kleitsa^a, K. Kawai^b, T. Shiotani^b, D.G. Aggelis^{a,*}

^a Department of Materials Science and Engineering, University of Ioannina, Ioannina 45110, Greece

^b Graduate School of Engineering, Kyoto University, Kyoto 615-8540, Japan

ARTICLE INFO

Article history:

Received 14 December 2009

Received in revised form

22 May 2010

Accepted 24 May 2010

Keywords:

Metal anchor head

Pre-stress

Interphase

Ultrasonics

Simulation

ABSTRACT

Pre-stressed strand wires embedded in a structure is a common way to reinforce the weak tensile nature of concrete or soil materials. Due to corrosion, the strands may lose the pre-tension with disastrous consequences. The accessibility to the strands is usually limited to the anchor head from where the assessment should be done. In this paper, through the thickness elastic wave simulations are conducted on the anchor head. The wave amplitude, transit time and other characteristics are influenced by the stress of the strand wires which affects the contact between wires, wedges and the surrounding matrix of the anchor head. The change of contact pressure between the strands and anchor head is simulated by modifying the rigidity of a model interphase material. The results are compared with experimental measurements on the same geometry of anchor head and different pre-stress levels. Therefore, a practical **nondestructive** inspection method to assess the pre-stress level of the strands is discussed.

© 2010 Published by Elsevier Ltd.

1. Introduction

Millions of ground anchorages have been installed over the past decades with relatively few recorded failures. However, as permanent anchorages in service become older, the subject is of growing importance, particularly for anchorages installed more than 30 years ago, many of which have been designed with corrosion protection considered inadequate by today's standard [1]. Initial tensile forces applied to pre-stressing strands undergo progressive time-dependent losses. These **pre-stress** losses, if unaccounted for, may cause catastrophic failures of pre-stressed concrete structures [2]. Despite their criticality, much research is still needed to develop techniques able to provide real-time information on the level of **pre-stress** in order to detect dangerous stress losses. Maintenance **testing** involves visual survey of the physical condition of the structure and the anchorages or measurement of the overall deformation and when applicable measurement of the load of selected tendons. The method to monitor the load of a tendon is the **so-called** "lift-off" method. However, it entails certain difficulties as it requires the anchor head to be raised by some millimeters using a hydraulic jack and therefore, may jeopardize the safety of the structure while only specific tendons can be examined [1]. Alternatively, X-rays can be applied [3] to visualize the interior; however this technique is time- and money- consuming while many precaution measures

for public and personnel health safety should be taken. Therefore, a fast, easy and safe inspection method which can confirm the satisfactory performance can extend the service life of anchored structures [1].

This study focuses on the ultrasonic method to evaluate the axial stress of the strands. Elastic waves have been used for the assessment of metal wires since their stress affects wave speed, dispersion parameters [2,4,5] as well as nonlinear behavior due to interwire interaction [6]. The ultrasonic method is already used for the measurement of the axial stress of steel bolts. According to the difference of length the axial force imposes, the transit time through the material can show the level of deformation and thus the axial stress. This technique did not produce reliable results for anchors installed deep into the ground because the propagation time depends not only on the anchor length but also on the boundary conditions of at the embedded end of the strand [7], the curvature of the tendon and the particular shape of the edge installed inside the ground [8]. In the present case, the assessment of the **pre-stress** of strands used for slope stability is attempted by measurements on the anchor head, which is the only accessible part. Due to the wedge geometry, as the pre-stress on the strands increases, the wedges obtain stiffer contact with the matrix material of the anchor. This has an effect on the overall rigidity of the anchor head. Therefore, longitudinal elastic waves are introduced in an anchor head and the time of flight, as well as the amplitude are measured for different levels of pre-stress. The experiment is numerically simulated by finite difference method software modeling the different quality of contact between wedges and the anchor head by means of an "interphase"

* Corresponding author. Tel.: +30 26510 08006; fax: +30 26510 08054.

E-mail addresses: daggelis@cc.uoi.gr, aggelis_d@yahoo.com (D.G. Aggelis).

material of varying elastic constants. Suitable wave parameters are sought for in order to yield a robust correlation with the applied stress on the tendons.

2. Experimental details

A typical example of a pre-stressed structure where the anchor heads are used to constrain the strand wires by means of wedges is shown in Fig. 1(a). As the pre-stress of the strand wires increases, the wedges obtain better contact with the anchor head, through the toughening of the interface between the wedges and their corresponding holes (Fig. 1(b)).

Fig. 2(a) shows a close-up of the anchor head with the strand wires and the wedges. Each wedge consists of 2 parts being placed around the strand wire, as shown in Fig. 2(b). Since there is no accessibility in the interior of the structure, the assessment should be conducted through the only area located in the surface, which is the anchor head. At the certain cross-section of the head (e.g. A-A of Fig. 1(a)) the ultrasound sensors can be applied, as seen in Fig. 2(c). Different pairs of longitudinal wave sensors were used with resonant frequency of 1, 5 and 7.5 MHz. In this paper the measurements of 1 MHz are presented, which were recorded with a sampling rate of 50 MHz. The height of the specific measurements is 30 mm below the large opening of the wedge holes (cross-section A-A).

The wave measurements were conducted on four different levels of increasing pre-stress, namely 0, 200, 400 and 600 kN while usually the maximum applied pre-stress on slope anchors is up to 500 kN. Results of time of flight and amplitude of the waves will be presented along with the numerical ones later. More experimental details can be found in [8].

3. Numerical simulations

The fundamental equation governing the two-dimensional propagation of elastic waves in a perfectly elastic medium, ignoring viscous losses is seen below:

$$\rho \frac{\partial^2 \underline{u}}{\partial t^2} = \mu \nabla^2 \underline{u} + (\lambda + \mu) \nabla \nabla \cdot \underline{u} \tag{1}$$

where $\underline{u} = u(x,y,t)$ is the time-varying displacement vector, ρ is the mass density, λ and μ are the first and second Lamé constants, respectively, while t is time. The focus, from the engineering point of view is given on simulating the actual cases examined experimentally and not on the numerical method itself. However, certain prerequisites should be followed in order for the analysis to lead to reliable results. The simulations were conducted with commercially available software [9] that solves the above equation in time domain with the finite difference method in the plane strain case. It operates by solving the above equation based on a method of finite differences. Eq. (1) is solved with respect to the boundary conditions of the object, which include the input source that has pre-defined time-dependent displacements at a given location and a set of initial conditions [10]. For heterogeneous media like the one studied herein, propagation in each distinct homogeneous phase is solved according to Eq. (1), while the continuity conditions for stresses and strains must be satisfied on the interfaces [10].

The basic geometry of the model is shown in Fig. 3. It corresponds to the cross-section A-A, of Fig. 1(a). The seven circles correspond to the holes made for the wedges and strand wires. The key parameter is the modeling of the contact between the anchor material and the wedges. This contact changes for different stress levels of the wires and therefore, this is a crucial parameter in the simulation. This condition is simulated by the addition of an interphase material with varying stiffness, as has

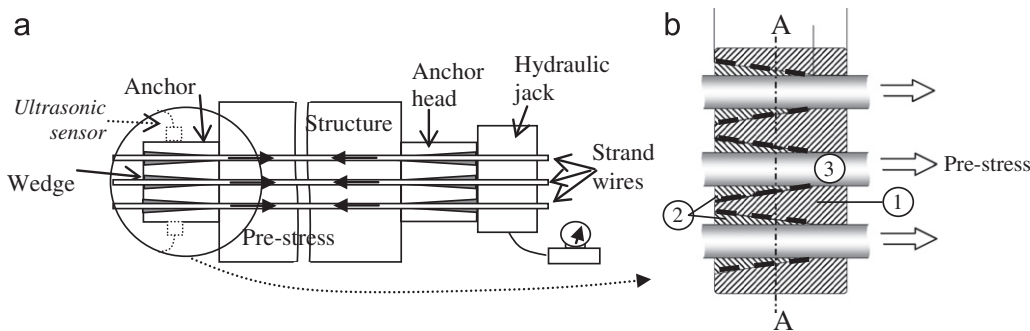


Fig. 1. (a) The basic geometry of pre-stressed structure. (b) Detail of the anchor head (1), including: wedges (2), and strand wires (3). The dashed line shows the contact “interphase” between the matrix and wedges.

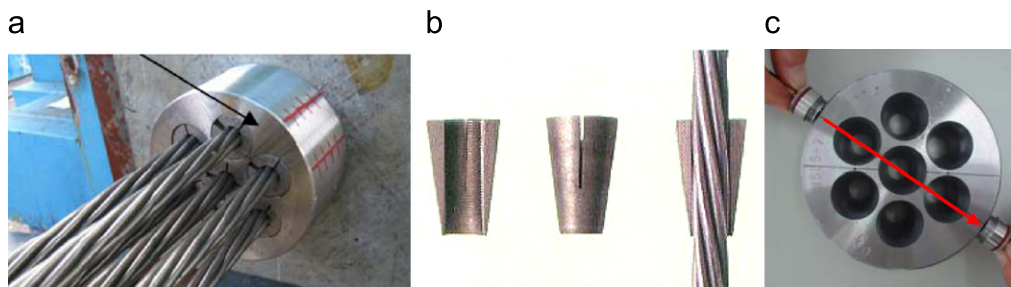


Fig. 2. (a) The anchor head with strand wires and wedges, (b) a close-up on the wedge and (c) photograph of the experiment on empty head.

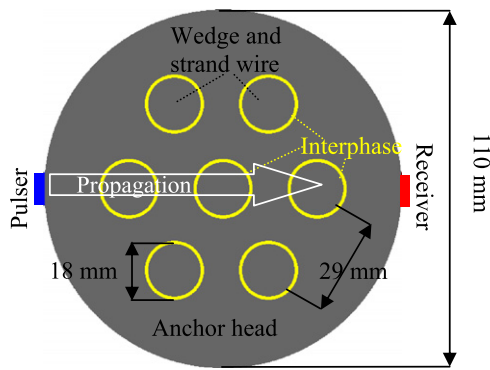


Fig. 3. Numerical geometric model corresponding to cross-section A-A of Fig. 2(a).

been studied for the case of surface cracks with faces in partial contact [11]. This is a practical way to simulate different contact cases between the matrix material and the wedge, since for the case of loose interphase (or when the interphase material obtains zero stiffness) no wave energy can propagate inside the wedge because of the strong reflection. On the opposite case, when the interphase obtains the stiffness of steel, it causes no scattering and the wave travels without obstruction. The thickness of the interphase layer is discussed below. For simplicity each of the seven strand wires was considered as one solid circle together with its surrounding wedge. The whole circular geometry was created inside a square of side 120 mm assigned properties of air, as is the actual experimental case. No boundary conditions were applied at the edges of this domain since the examined time window is not enough for any reflection from the edges of the domain to the receiver.

Materials were considered elastic without viscosity components. The mechanical properties of the matrix anchor head, the wedge and the strand wire are equal to steel's, with Young's modulus 205 GPa, Poisson's ratio of 0.3 and density of 7800 kg/m³ resulting in a longitudinal wave velocity, C_p , of 5948 m/s. The interphase material's velocity was varied to different values starting from 330 m/s which simulates the case of negligible contact (air). Then, by adjusting the elastic properties of the interphase, the velocity, C_p , was set to the values 1000, 2000, 3000, 4000 and 5000 m/s and 6000 m/s. The last value simulates the case in which the interphase is as rigid as the steel anchor head, wedges and strand wires.

The "pulsar" introduced a displacement excitation of 1 cycle of 1 MHz vertical to the surface. The receiver provided the average vertical displacement on its whole length (10 mm), meaning that the obtained waveform was the average of the vertical displacement of the surface nodes on the length of the receiver.

Concerning the mesh size, a preliminary evaluation took place to select a suitable value for time-efficient as well as accurate simulation. The mesh sizes applied were from 5 mm down to 0.8 mm and the corresponding transit times of the first detectable disturbance on the receiver for the case of loose interphase ($C_p=330$ m/s) were calculated for each case. The results are seen in Fig. 4(a), while in Fig. 4(b) the waveforms obtained for the 5 mm mesh and 1 mm mesh are depicted. The waveforms show no significant difference, while the transit times seem to converge as the mesh size becomes finer. The extrapolated value of the transit time for infinitely fine mesh is 18.562 μ s. The simulations were conducted with the mesh size of 3 mm, which resulted in considerable accuracy, (18.43294 μ s, deviation only 0.7% from the extrapolated value) while it was acceptable in terms of time consumption. The time step was 0.00696 μ s while the typical period of the wave excited was 1 μ s (for frequency 1 MHz).

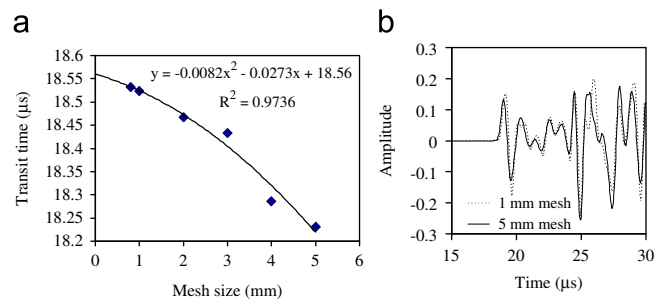


Fig. 4. (a) Transit time results for different mesh size and (b) waveforms obtained for two different mesh sizes.

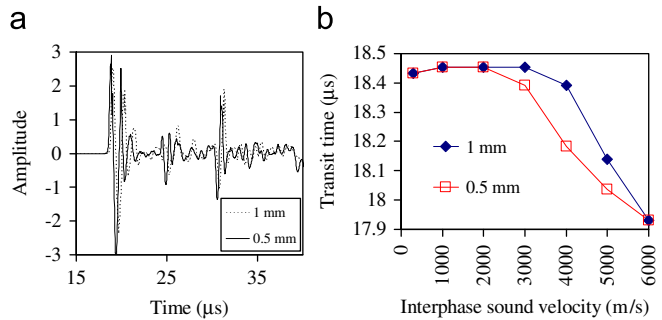


Fig. 5. (a) Simulated waveforms for two different interphase thicknesses and $C_p=4000$ m/s, and (b) transit time vs. interphase stiffness curves for two different interphase thicknesses.

As mentioned above, the mechanical properties of the interphase were defined in such a way to simulate the different degree of contact of the wedge to the matrix. The two marginal cases are the one of no contact, assigned to the rigidity of air for the simulation, and maximum contact, corresponding to the stiffness of steel. However, there is no physical value a priori suitable for the thickness of the interphase material. The initially applied value was 1 mm but the value of 0.5 mm was also applied in order to examine the effect of this modeling parameter. Indicatively, Fig. 5(a) contains the responses of the receivers recorded for both cases and for the same interphase stiffness ($C_p=4000$ m/s). From the shape of the waveforms, as well as, from the transit time diagrams (Fig. 5(b)) it is concluded that the interphase layer thickness is not a crucial parameter for the range below 1 mm. The results presented hereafter were produced by the thickness of 0.5 mm. It is mentioned that the results for low interphase stiffness are independent of the layer thickness. This is reasonable because the thickness was changed by adjusting the internal diameter of the layer, since in an actual condition the wedge will be restrained by the solid anchor head. Thus, for "loose" interphase the entire wedge circle acts as a cavity and no energy propagates inside. Therefore, the thickness of the interphase layer does not influence the propagation at all. On the opposite case of maximum stiffness, the wave propagates in a straight line as if no interphase exists and therefore, again the interphase layer thickness is not significant. Fig. 5(b) shows that the interphase thickness as a simulation parameter can influence the results by maximum 1.15% but not for the marginal cases of no and maximum contact.

4. Wave amplitude and transit time

In Fig. 6(a) and (b) two snapshots of the transient displacement field for the moments of 4.5 and 15 μ s are included for the case

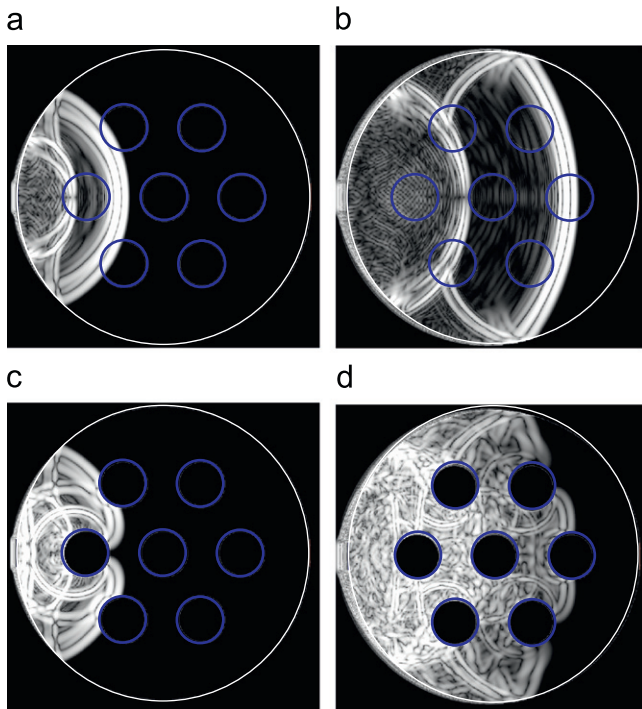


Fig. 6. Snapshots of the displacement field, (a) and (b) for stiff interphase ($C_p=6000$ m/s), (c) and (d) for weak interphase ($C_p=330$ m/s).

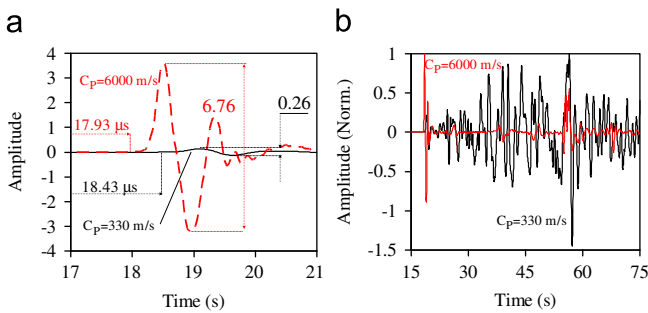


Fig. 7. (a) First arrivals of the longitudinal wave for two different levels of interphase stiffness and thickness of 0.5 mm. (b) The same waveforms up to 75 μ s, normalized to their positive maximum.

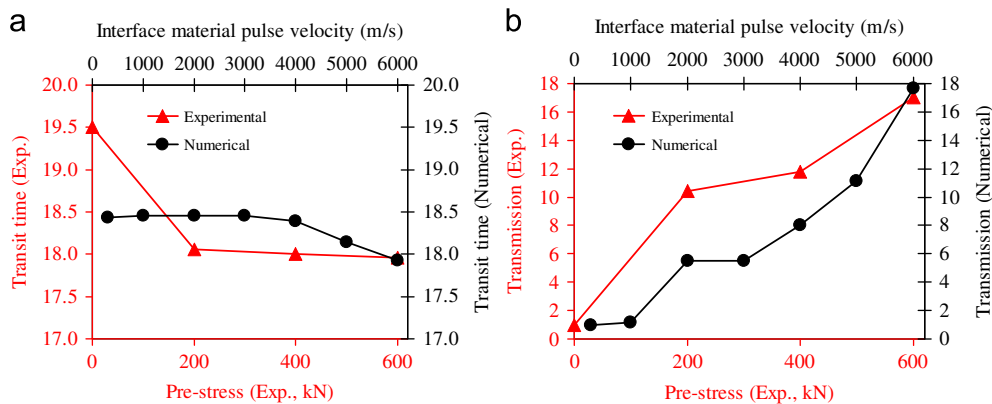


Fig. 8. (a) Experimental transit time vs. pre-stress and numerical transit time vs. interphase C_p . (b) Experimental wavefront amplitude vs. pre-stress and numerical amplitude vs. interphase C_p .

where the interphase exhibits the stiffness of steel (long. velocity 6000 m/s). The wavefront is not scattered since the mechanical impedance does not change throughout the straight wave path. The cross section behaves as a homogeneous circle. On the other hand when the interphase is considered similar to air (see Fig. 6(c) and (d)), the wavefront is scattered and the straight path cannot be followed by the wave.

Fig. 7(a) shows the initial part of the simulated waveforms for the two cases of loose and stiff interphase. The stiff interphase ($C_p=6000$ m/s) results in definitely higher amplitude than the loose ($C_p=330$ m/s). The later is the result of multiple scattering of the wavefront on the circular wedges. Actually, since the stiffness in the loose case, corresponds to air, the wedges act like holes, breaking and multiply scattering the wavefront. It is thus reasonable that the energy propagating in the forward direction is much less than the stiff case. There is also a visible delay in transit time (approximately 0.5 μ s) due to the obstructed linear forward path. The transit time is measured by the first detectable disturbance of the waveforms. In order to highlight the multiple scattering that occurs in the case of loose interphase, Fig. 7(b) shows the waveforms for a long duration, normalized to their maximum. It is characteristic that for the loose interphase, the energy is distributed over the whole duration, due to the multiple scattering on each "hole" and the maximum amplitude is observed after 50 μ s. On the other hand for the stiff interphase almost all the energy arrives before 20 μ s, since there is no scattering inside the geometry, but only reflections from the circular boundary.

Below one can see numerical results of transit time for different stiffness of the interphase (see Fig. 8(a)). The transit time is approximately constant until the interphase obtains stiffness corresponding to longitudinal velocity of 4000 m/s. When the interphase rigidity increases, the transit time is shortened. This maximum difference is 0.5 μ s and can be measured by any compatible ultrasonic setup, corresponding to a difference of 2.7%. This behavior shows that when the interphase is below some threshold stiffness (corresponding to material velocity of 4000 m/s), even though some energy propagates through, still the part of the energy trailing around the wedges arrives earlier. However, when the interphase obtains stiffness similar to the matrix material itself (steel) then the straight path is followed resulting in shorter transit time.

On the same figure (Fig. 8(a)) one can see the experimental results for the frequency of 1 MHz. When no pre-stress is applied, the transit time is measured at 19.50 μ s. As the pre-stress is increased to 200 MPa the transit time is shortened considerably to

18.06 μs and stays approximately constant until the final load of 600 MPa (17.96 μs). The decrease for the experimental measurement is almost 8%, being more sensitive though between zero and the low pre-stress level of 200 kN.

The wave transit time measurement although is one of the most fundamental ones in **nondestructive** testing, it is not always the most sensitive to the internal condition of the materials. Especially for inhomogeneous materials, where strong scattering interactions are expected, other parameters related to the transmission or energy of the wave are more appropriate [12]. In this case, in order to examine energy-related features, the amplitude of the first cycle of the received wave was measured. Assuming that no viscous components are included, the whole amount of energy excited by the pulser will eventually reach the transducer as it is trapped in the metal anchor head surrounded by air. However, the first cycle will contain only the forward scattered components and the rest of the energy will arrive later, especially when strong scattering occurs. Thus, the first cycle is more sensitive to the presence of internal scatterers.

The numerical amplitude of the first cycle for different interphase stiffness is depicted in Fig. 8(b) normalized to the amplitude of zero stiffness. It is evident that as the interphase gets stiffer, the **wavefront** continuously exhibits increasing amplitude until it becomes 18 times higher than the initial value. Again on the same figure the experimental results are depicted. The amplitude of the first cycle increases strongly as the loading is building up, reaching approximately the same value as the numerical result.

It is seen that the results of both amplitude and transit time for the maximum load almost coincide with the numerical of the highest interphase stiffness (level of steel). This shows that when the maximum load (600 kN) is applied in practice, the whole anchor head behaves as one homogeneous geometry, validating the selection of $C_p=6000$ m/s for the interphase. In this case, due to the strong contact, the propagating wave will not “see” any interphase, meaning that the transit time corresponds to the one in a rigid steel circular geometry. When the transit time is increased this should be considered an alarm for relaxation. For the case of no pre-stress, the experimental amplitude is again close to the simulation using the “loose” interphase, implying that the selection of 330 m/s for the velocity of the poor contact is again valid. The correlation between the whole range of possible pre-stress loads and “interphase” velocities may be linear, exponential or any other form but this cannot be confirmed so far. The results show that the chosen interphase velocities result in better agreement for the minimum and maximum pre-stress than the intermediate loads of 200 and 400 kN. Making more experimental measurements as well as checking more parameters, potentially more sensitive to the contact, will

hopefully establish stronger agreement. In any case, since the trend for amplitude is monotonic it seems that amplitude parameters of the received wave are promising features for further study. Additionally, although the transit time is influenced only by 3%, it is still indicative of the stiffness of the stressed anchor.

5. Discussion

5.1. Other descriptors

The shape of the propagating wave inside a material depends on the inhomogeneity it contains. For cases where the material is homogeneous the obtained waveforms are very close to the excited signal. This is because the energy travels in a straight path and all energy components arrive at the same time. However, when scattering mechanisms are active, the energy is divided to different wave paths with various lengths. Some of the components may propagate in a straight or approximately straight line; however, most of the energy will be strongly scattered and thus will arrive later and in a longer time span. This can be clearly seen by the shape of the rectified waveforms for the different cases, as shown in Fig. 9(a) where the “loose” interphase waveform exhibits several peaks stronger than the initial throughout the duration up to 45 μs. On the contrary, the stiff interphase waveform exhibits negligible later arrivals compared to the initial forward propagating component of arriving at 18 μs.

Calculating the center of gravity of the envelope on the time axis, results in Fig. 9(b) which presents a quite strongly linear relation between the interphase stiffness and the center of gravity, A_T , of the rectified signal envelope, defined similarly to [13]

$$A_T = \frac{\int t \cdot W(t) dt}{\int W(t) dt} \tag{2}$$

where t is time and $W(t)$ is the rectified time signal.

The arrival of the major energy components is monotonically translated to the front of the waveform as the contact between the anchor and the wedges becomes stiffer. Therefore, this is another reliable parameter that could be utilized, since the whole waveform can be recorded and analyzed.

The arrival of the major energy components can be well visualized by the use of wavelets. Wavelet transformation is a means of conducting frequency analysis in a localized part of a signal. Therefore, it is possible to identify the time within a waveform when each frequency component is active (as opposed to the Fourier transform that gives information about the frequency content of the whole signal as an entity). The wavelet

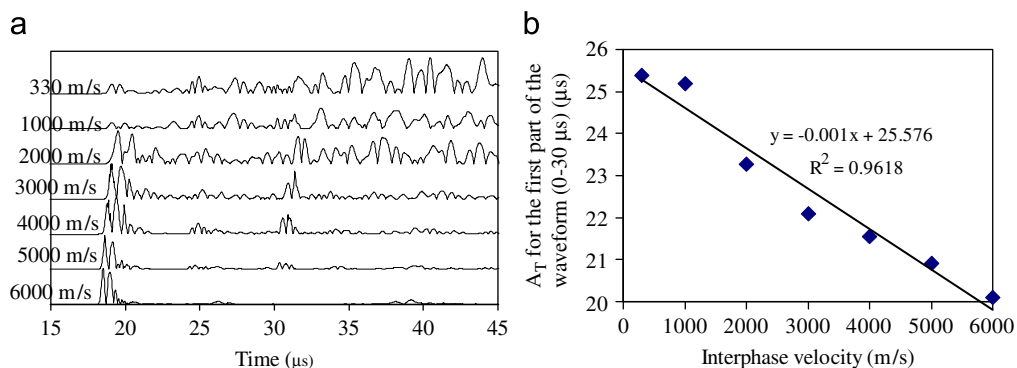


Fig. 9. (a) Rectified waveforms corresponding to different interphase velocities (arbitrary vertical axis). (b) Center of gravity of the time waveforms for different interphase stiffness.

transform (WT) works by breaking the signal into shifted and scaled versions of the original wavelet (fast decaying mathematical function) [14]. To handle suitably any signal, different

original (“mother”) wavelet functions can be used. In the specific case, the software used [15] employs the “Gabor” Wavelet, which has proven useful for analysis of elastic wave signals [16].

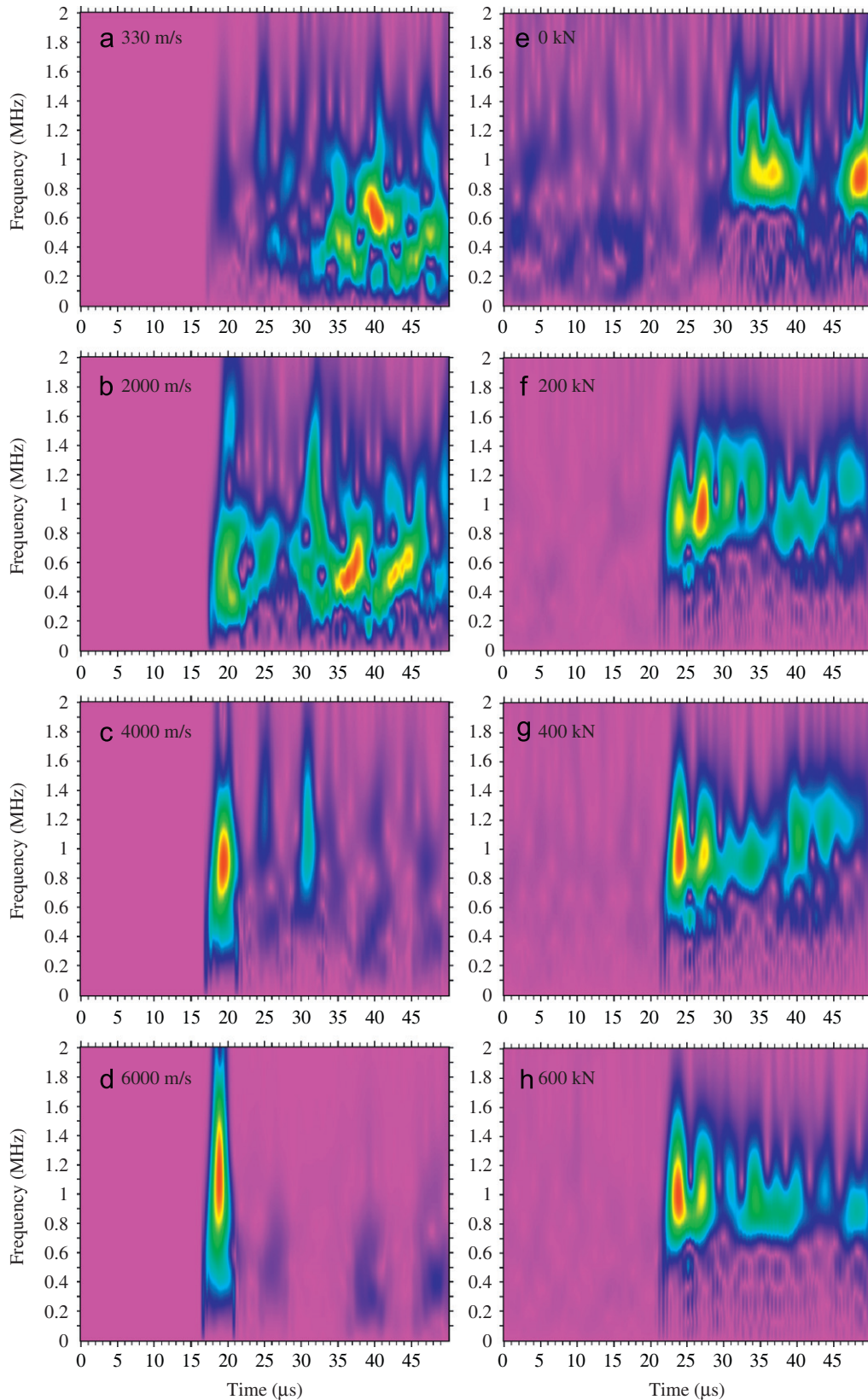


Fig. 10. (a)–(d) Wavelet transformation of the simulated longitudinal wave responses for different interphase stiffnesses and (e)–(h) wavelet transformation of the experimental longitudinal wave response for different pre-stress levels.

Fig. 10(a)–(d) show the wavelet transformation of four simulated waveforms corresponding to different interphase sound velocities. For the loose interphase the major components arrive later than 35 μs, much later than the initial arrivals, due to multiple scattering. As the interphase becomes stiffer, the intensity of the energy is translated to the front while for the case of steel stiffness the rest of the energy is negligible (Fig. 10(d)). Another important piece of information supplied by the wavelets, additionally to the time translation of energy, is the frequency content. For high stiffness the major part of energy is centered around 1 MHz (Fig. 10(d)). However, for loose interphase, the center of frequency decreases to 500 kHz or less (Fig. 10(a)). The downshift of frequencies is common for wave propagation in inhomogeneous materials due to the fact that scattering attenuation is stronger for higher frequencies [12,17]. It seems that the frequency content can supply another important descriptor to characterize the quality of the interphase.

The trend exhibited in the simulated results, was also examined in the experimental results, as seen in Fig. 10(e)–(h). The trend is similar since the burst of energy is translated to the front as the pre-stress is increased. It is suggested therefore, that the visual inspection of the wavelet transformation can provide the initial information about the contact condition in the anchor head. It is mentioned that the four cases depicted in Fig. 10(a)–(d) are selected for their increasing order of stiffness and do not necessarily correspond to the pre-stress of Fig. 10(e)–(h).

5.2. Shear waves

One of the goals of simulation is to support the experimental results and help in the understanding of the complicated phenomena that take place in an inhomogeneous structure. Another is to propose new features for more accurate characterization. Any experiment always depends on the specific equipment. Simulation is a reliable way to expand to different conditions. In the particular case, as mentioned earlier, the experiment was conducted by P-wave transducers, meaning that the excitation was a displacement vertical to the surface, and the response was the transient vertical displacement on the receiver placed on the opposite side. However, in inhomogeneous materials, which entail multiple scattering, shear waves are also generated each time the wavefront impinges in an inhomogeneity [18]. Although the incident wave is longitudinal, the scattered field includes both longitudinal and shear components since a part of energy is mode-converted. The amount of longitudinal wave energy which is converted to shear wave depends on the impedance mismatch between the matrix and the embedded inhomogeneity. In the present case, this conversion depends on

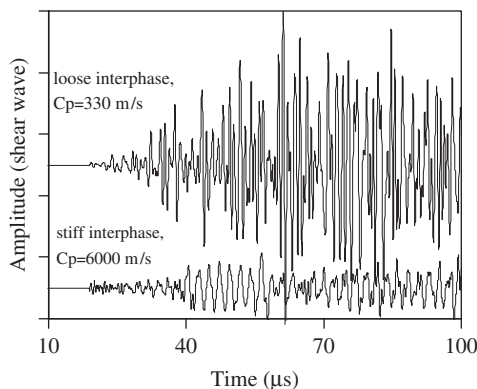


Fig. 11. Typical simulated waveforms obtained with shear transducer for two different levels of interphase stiffness.

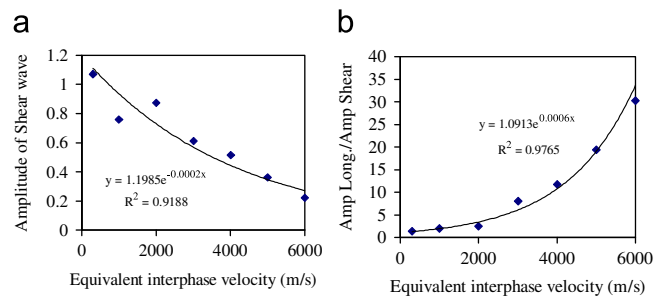


Fig. 12. (a) Shear wave amplitude and (b) ratio of longitudinal to shear wave amplitude for different levels of interphase stiffness.

the properties of the interphase. The shear wave (displacement components parallel to the sensor surface) can be readily obtained in the simulation. One example is depicted in Fig. 11, where the shear waves obtained from the simulation for the two marginal cases of loose and stiff interphases are depicted. The energy of the shear waveform for the loose interphase is much higher than the case of stiff interphase. The shear amplitude increases inversely to the stiffness of the interphase, see Fig. 12(a). Considering that as inhomogeneity increases, the mode conversion is increased and that more of the P-wave energy is converted to shear, the ratio of longitudinal amplitude to shear proves a very sensitive tool for the assessment, as seen in Fig. 12(b). The ratio of the amplitudes of the whole P-waveform to S-waveform is 1.35 for the loose interphase when more energy is converted to shear waves. However, when the anchor behaves homogeneously, this ratio becomes more than 30, since almost no mode conversion occurs. The correlation coefficient R² is almost 0.98, showing that this parameter is very robust to include in the NDT characterization armory for the specific application, provided that suitable and repeatable coupling conditions can be assured for shear wave transducers. Therefore, it is suggested by the simulations that although powerful parameters can be obtained from P-waves, the combined use of shear transducers could certainly enhance the characterization.

6. Conclusion

The study presented herein concerns the nondestructive evaluation of the pre-stress in metal strand wires used for slope stability. Due to the wedge geometry, increased pre-stress enhances the contact of the metal parts and this has an effect on the propagation of elastic waves through the head, as exhibited by the change of transit time and amplitude. Numerical simulations on the exact geometry exhibit a similar trend for transit time and amplitude of the wavefront, showing that when the maximum level of pre-stress is applied (600 kN), the interphase is as stiff as the steel material itself. The study should continue in order to firmly match the stiffness of the model “interphase” material to the actual pre-stress applied on the strand wires by the combination of simulations and experiments.

The use of wavelets helps to quickly assess the condition of the anchor head, while all the parameters that change monotonically with the applied load, could be included in a multi-variate approach to increase the characterization power. Further ideas include the use of shear wave transducer either as receiver to record the mode-converted energy or as both pulser and receiver since shear waves show greater sensitivity to the existence of interphases. The shortcoming of this approach is that experimentally, the transmission of shear waves into the specimen is much more difficult and special care should be taken of the acoustic coupling conditions. Apart from the indicative wave parameters

discussed herein (amplitude, transit time, delayed wave arrivals) several others should be tested, like the transmitted frequency which strongly depends on scattering on the wedges. Finally, another suggestion includes the excitation of elastic waves on each strand wire directly and receiving by a point on the anchor head so that assessment of the load at each wire separately can be achieved.

References

- [1] Littlejohn S, Mothersille D. Maintenance testing and service behaviour monitoring of permanent ground anchorages, In: Littlejohn editor. Ground anchorages and anchored structures in service, 2007; i-xxxvi.
- [2] Chen RHL, Wissawapaisal K. An ultrasonic method for measuring tensile forces in a seven-wire prestressing strand, Quantitative Nondestructive evaluation. AIP Conference Proceedings 2002;615:1295-302.
- [3] Mitchell TM. Radioactive/nuclear methods. In: Malhotra VM, Carino NJ, editors. CRC handbook on nondestructive testing of concrete. Florida: CRC Press; 1991. p. 227-52.
- [4] Washer GA, Green RE, Pond Jr. RB. Velocity constants for ultrasonic stress measurement in prestressing tendons. Research in Nondestructive Evaluation 2002;14:81-94.
- [5] Chaki S, Bourse G. Guided ultrasonic waves for non-destructive monitoring of the stress levels in prestressed steel strands. Ultrasonics 2009;49:162-71.
- [6] Bartoli I, Phillips R, Di Scalea FL, Salamone S, Coccia S, Sikorsky CS. Load monitoring in multiwire strands by interwire ultrasonic measurements. Proceedings of SPIE—The International Society for Optical Engineering 2008;6932. Article number 693209. 25
- [7] Madenga V, Zou DH, Zhang C. Effects of curing time and frequency on ultrasonic wave velocity in grouted rock bolts. Journal of Applied Geophysics 2006;59(1):79-87. 27
- [8] Kawai K, Shiotani T, Ohtsu H, Yanase T, Tanaka H. Estimation of axial stress in ground anchors by using ultrasonic technique, In: Proceedings of the EIT-JSCE, Geotechnical infrastructure management, (in CD, 9), 2009. 29
- [9] Wave 2000, Cyber-Logic, Inc., NY (<http://www.cyberlogic.org>). 31
- [10] Kaufman JJ, Luo G, Siffert RS. Ultrasound simulation in bone, IEEE transactions on ultrasonics. Ferroelectrics and Frequency Control 2008;55(6):1205-18. 33
- [11] Pecorari C. Scattering of a Rayleigh wave by a surface-breaking crack with faces in partial contact. Wave Motion 2001;33:259-70. 35
- [12] Edwards RS, Dixon S, Jian X. Characterization of defects in the railhead using ultrasonic surface waves. NDT & E International 2006;39(6):468-75. 37
- [13] Aggelis DG, Philippidis TP. Ultrasonic wave dispersion and attenuation in fresh mortar. NDT & E International 2004;37(8):617-31. 39
- [14] Misiti M, Misiti Y, Oppenheim G, Poggi J. 1996. Matlab Wavelet 490 Toolbox User's Guide. 39
- [15] AGU-Vallen Wavelet, R2005.1121, www.vallen.de. 41
- [16] Aggelis DG, Shiotani T, Kasai K. Evaluation of grouting in tunnel lining using impact-echo. Tunnelling and Underground Space Technology 2008;23: 629-37. 43
- [17] Shiotani T, Aggelis DG. Wave propagation in concrete containing artificial distributed damage. Materials and Structures 2009;42(3):377-84. 45
- [18] Graff KF. Wave motion in elastic solids. New York: Dover Publications; 1975. 45